

ULRR

Self-standing 3D core-shell nanohybrids based on amorphous Co-Fe-Bi nanosheets grafted on NiCo₂O₄ nanowires for efficient and durable water oxidation

Item Type	Article
Authors	Suryawanshi, Umesh P.;Suryawanshi, Mahesh P.;Ghorpade, Uma V.;He, Mingrui;Lee, Dongmin;Shin, Seung Wook;Kim, Jin Hyeok
Citation	ACS Applied Energy Materials; 3 (5), pp. 4338-4347
Publisher	American Chemical Society
Download date	2026-03-17 06:21:02
Item License	https://creativecommons.org/licenses/by-nc-sa/1.0/
Link to Item	https://hdl.handle.net/10344/8778

Self-Standing 3D Core-Shell Nanohybrids Based on Amorphous Co-Fe-B Nanosheets Grafted on NiCoO Nanowires for Efficient and Durable Water Oxidation

Umesh P Suryawanshi, Mahesh P. Suryawanshi, Uma V. Ghorpade, Mingrui He, Dongmin Lee, Seung Wook Shin, and Jin Hyeok Kim

ACS Appl. Energy Mater., **Just Accepted Manuscript** • DOI: 10.1021/acsaem.0c00040 • Publication Date (Web): 10 Mar 2020

Downloaded from pubs.acs.org on March 16, 2020

Just Accepted

“Just Accepted” manuscripts have been peer-reviewed and accepted for publication. They are posted online prior to technical editing, formatting for publication and author proofing. The American Chemical Society provides “Just Accepted” as a service to the research community to expedite the dissemination of scientific material as soon as possible after acceptance. “Just Accepted” manuscripts appear in full in PDF format accompanied by an HTML abstract. “Just Accepted” manuscripts have been fully peer reviewed, but should not be considered the official version of record. They are citable by the Digital Object Identifier (DOI®). “Just Accepted” is an optional service offered to authors. Therefore, the “Just Accepted” Web site may not include all articles that will be published in the journal. After a manuscript is technically edited and formatted, it will be removed from the “Just Accepted” Web site and published as an ASAP article. Note that technical editing may introduce minor changes to the manuscript text and/or graphics which could affect content, and all legal disclaimers and ethical guidelines that apply to the journal pertain. ACS cannot be held responsible for errors or consequences arising from the use of information contained in these “Just Accepted” manuscripts.

1
2
3
4
5 **Self-Standing 3D Core-Shell Nanohybrids Based on**
6
7
8 **Amorphous Co-Fe-B_i Nanosheets Grafted on NiCo₂O₄**
9
10
11 **Nanowires for Efficient and Durable Water Oxidation**
12
13
14

15
16 *Umesh P. Suryawanshi,^{a,‡} Mahesh P. Suryawanshi,^{*,b,‡} Uma V. Ghorpade,^c Mingrui He,^b*
17
18 *Dongmin Lee,^a Seung Wook Shin,^{*,d} and Jin Hyeok Kim^{*,a}*
19
20

21 ^aOptoelectronics Convergence Research Center and Department of Materials Science and
22 Engineering, Chonnam National University, 300, Yongbong-Dong, Buk-Gu, Gwangju 61186,
23 South Korea
24
25
26
27

28
29 ^bSchool of Photovoltaic and Renewable Energy Engineering, UNSW Sydney, Sydney, NSW
30 2052, Australia
31
32

33
34 ^cDepartment of Chemical Sciences and Bernal Institute, University of Limerick, Limerick, V94
35 T9PX, Ireland
36
37

38
39 ^dFuture Agricultural Research Division, Water Resource and Environment Research Group,
40 Rural Research Institute, Korea Rural Community Corporation, Ansan-Si, Gyeonggi-do 15634,
41 South Korea
42
43
44
45

46
47 **KEYWORDS.** Co-Fe-B_i/NiCo₂O₄/NF; 3D core-shell nanohybrid structure; water oxidation; one-
48 step solution process; electrocatalysts.
49
50
51
52
53
54
55
56
57
58
59
60

1
2
3 ABSTRACT. Here, three-dimensional (3D) core-shell nanohybrid based on few-layer amorphous
4 Co-Fe-B_i nanosheets directly grown on crystalline NiCo₂O₄ nanowires supported on Ni foam (Co-
5 Fe-B_i/NiCo₂O₄/NF) are facilely fabricated as highly efficient and durable electrocatalysts for water
6 oxidation. This self-standing 3D core-shell nanohybrid design with unique materials chemistry and
7 excellent interface engineering enhance the mass transport and stimulates the production of active
8 sites during OER. Serving as the anode catalysts, the resulting self-standing Co-Fe-B_i/NiCo₂O₄/NF
9 nanohybrid electrocatalysts show better electrocatalytic activity with an overpotential of 227 mV at
10 10 mA/cm², a Tafel slope of 45 mV dec⁻¹, excellent durability over 40 h, and the ability to deliver a
11 current density of 200 mA/cm² at an overpotential of ~ 410 mV in an alkaline medium. Thus, the
12 excellent electrocatalytic performance of Co-Fe-B_i/NiCo₂O₄/NF nanohybrid demonstrates the
13 importance of design and development of core-shell nanohybrids for large-scale practical
14 applications in a multitude of energy-conversion devices.
15
16
17
18
19
20
21
22
23
24
25
26
27
28
29
30

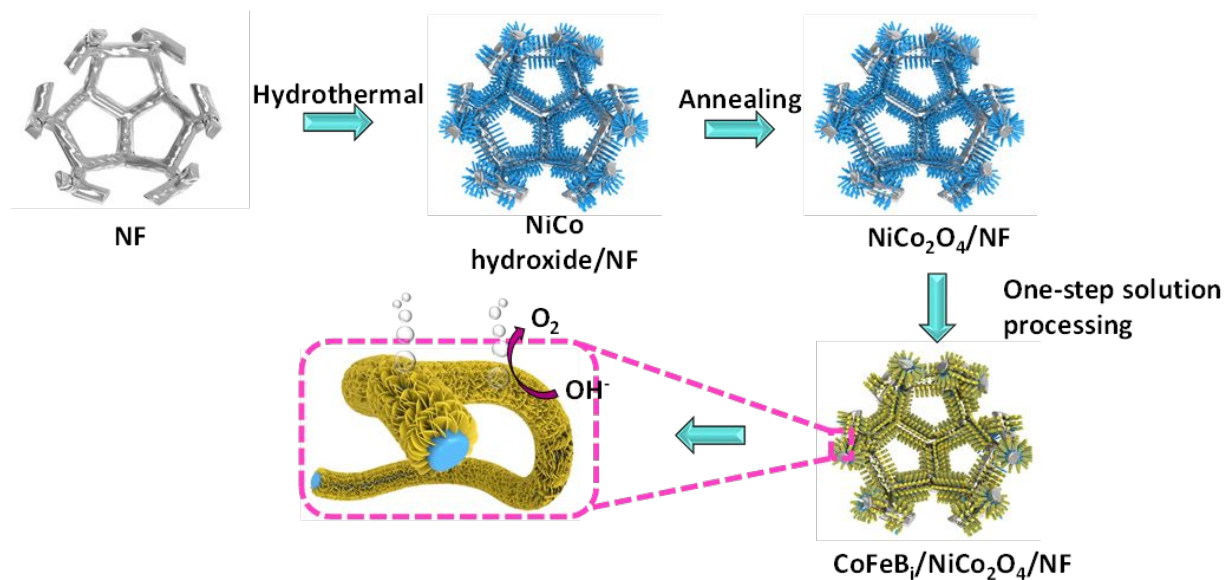
31 INTRODUCTION

32
33
34 Electrolytic splitting of water into hydrogen fuels is widely considered the most advanced
35 technology for clean, sustainable and environmentally friendly hydrogen production and
36 storage.^{1,2} However, the present bottleneck impeding the overall water splitting efficiency is the
37 oxygen evolution reaction (OER) due to its sluggish kinetics resulting from the multiple proton-
38 coupled electron transfer process.³⁻⁵ Accordingly, the OER imposes a considerable overpotential
39 requirement in electrolytic water splitting compared to that of the hydrogen evolution reaction
40 (HER), even when facilitated by high catalytic activity and precious IrO₂ and RuO₂
41 electrocatalysts.⁶⁻¹⁰ The electrocatalysts for the OER therefore must be able to accommodate the
42 requirements of the OER for large-scale applications, such as earth-abundancy, low-cost, high
43 durability and high electrocatalytic activity.^{4,5}
44
45
46
47
48
49
50
51
52
53
54
55
56
57
58
59
60

1
2
3 In this context, several classes of metal-based electrocatalysts for the OER have been
4 developed, including metal oxides and hydroxides,^{11,12} as well as non-metal-based OER
5 electrocatalysts.¹³ Remarkably, recent studies have demonstrated a significant improvement in
6 the OER activity by incorporating non-metal elements (e.g., N, S, Se, P) in these oxide, or
7 hydroxide compounds,^{3,10,14–18} and the improvement has been attributed to the modified
8 electronic structures and efficient charge transfer between the metal-metalloid structures.¹⁹ These
9 developments have led to further exploration of the applications of the rarely studied metal
10 borates, which is reasonable since the borate species in the metal borate share certain properties
11 with the aforementioned metal-metalloids and also exhibits high durability and catalytic
12 efficiency.²⁰ In this regard, few studies on the development of monometallic cobalt borate (Co-
13 B_i)^{21,22} and nickel borate (Ni-B_i)^{4,23} electrocatalysts for the OER have been reported with
14 catalytic activity far below that of the state-of-the-art electrocatalysts. We have recently
15 demonstrated, for the first time, the facile solution processing of amorphous Co-Fe-B_i nanosheets
16 directly on a porous Ni foam (NF) as electrocatalyst²⁴ which exhibited better electrocatalytic
17 activity than that of its monometallic counterpart, thanks to the synergy between the Co and Fe
18 elements and the abundant defect sites.^{24,25} Although efficient and durable electrocatalysts have
19 been developed, the rational design of the electrocatalyst architecture is considered to be an
20 effective approach to further improve the electrocatalyst performance. Three-dimensional (3D)
21 crystalline core-amorphous shell hybrid nanoarchitecture directly grown on the conductive
22 supports is of particular interest due to its large surface area, fast mass transport abilities,
23 exposing maximal catalytically active sites and intimate access to the electrolyte.^{26,27} Few
24 attempts have been made to develop 3D core-shell nanoarchitecture electrocatalysts based on
25 transition metal borate compounds, most of them are using in-situ electrochemical surface
26
27
28
29
30
31
32
33
34
35
36
37
38
39
40
41
42
43
44
45
46
47
48
49
50
51
52
53
54
55
56
57
58
59
60

1
2
3 amorphization process.²⁸⁻³² Some interesting results were obtained, however, these in situ-
4
5 formed active metal borate shell are likely to mispair with the underlying core structure due to
6
7 the poor OER activity in near-neutral and alkaline media. Therefore, the rational design of an
8
9 alternative 3D core-shell nanoarchitecture based on Co-Fe-B_i with abundant active sites on the
10
11 self-standing highly conductive scaffolds for water oxidation is of great significance.
12
13

14
15 Based on these motivations, we demonstrate the design and development of 3D strongly
16
17 coupled core-shell nanohybrids, in which two-dimensional (2D) amorphous Co-Fe-B_i nanosheets
18
19 are easily integrated on the one-dimensional (1D) crystalline NiCo₂O₄ nanowires on the porous
20
21 NF. Specifically, a few layers of Co-Fe-B_i nanosheets are uniformly grown using one-step
22
23 solution processing on the surface of hydrothermally grown NiCo₂O₄ nanowires that are ~ 150
24
25 nm in diameter and a few micrometers in length and are perpendicular to the NF. The motif of
26
27 the 3D core-shell nanohybrid can be summarized as follows: i) open channels of highly porous
28
29 NF allows the growth of the core-shell nanoarchitecture, which further enhances the specific
30
31 surface area without affecting the gas bubble dissipation of the NF,³³ ii) earth-abundant,
32
33 environmentally friendly and low-cost NiCo₂O₄ nanowires provide pathways for efficient
34
35 electron transport due to their excellent electrical conductivity,^{34,35} iii) amorphous Co-Fe-Bi
36
37 nanosheets exposes abundant catalytically active sites,²⁴ and iv) 3D strongly coupled three-level
38
39 nanohybrids offer large surface area with maximal exposure of the active sites and access to the
40
41 electrolyte.³³ As a result, this 3D core-shell Co-Fe-B_i/NiCo₂O₄/NF nanohybrid boosts the
42
43 electrocatalytic activity in an alkaline medium. Notably, the performance of the 3D core-shell
44
45 Co-Fe-B_i/NiCo₂O₄/NF nanohybrid in the present study outperforms among the borate-based
46
47 electrocatalysts and ranks among the most active transition metals-based electrocatalysts for
48
49 alkaline water oxidation (Table S1).
50
51
52
53
54
55
56
57
58
59
60



Scheme 1. Schematic illustration of the fabrication procedures of the self-standing 3D core-shell Co-Fe-B_i/NiCo₂O₄/NF nanohybrid electrocatalysts.

RESULTS AND DISCUSSION

The schematic diagrams and photographs in Scheme 1 and S1 illustrate the facile two-step approach for preparing the 3D core-shell nanohybrid electrocatalysts on the highly porous NF (denoted as Co-Fe-B_i/NiCo₂O₄/NF). The NF, with interconnected macropores offering large specific surface area, mechanical robustness and high electrical conductivity, was used as a self-supported substrate (Figure S1a). Vertically aligned NiCo₂O₄ nanowires were grown on the NF substrate via a low-temperature hydrothermal method at 120 °C for 6 h followed by annealing at 400 °C for 3 h for crystallization.³⁶ A hydrothermal reaction led to the formation of brown thin film of NiCo-based hydroxides (Figure S1b), which turned black as a result of crystallization to NiCo₂O₄ after the annealing treatment (Figure S1c). A few layers of Co-Fe-B_i nanosheets were deposited as a shell on the NiCo₂O₄ nanowire core using one-step solution processing adopted from our previous work.²⁴ This facile solution processing did not significantly change the color

1
2
3 of the electrode, indicating that the Co-Fe-B_i shell was ultrathin and/ or few layers thick and
4 transparent (Figure S1d). Figure S2 shows that the NF has an interconnected open network
5 structure with a pore size of hundreds of micrometers, making it a legitimate candidate as a
6 scaffold support for the electrocatalyst deposition. Moreover, the large, open and porous
7 structure of the NF facilitated the mass transport of the reactant hydroxide ions and rapid
8 dissipation of bubble formation and gaseous products (H₂ and O₂).³⁷

9
10
11
12
13
14
15
16
17 Figure 1a shows the field emission scanning electron microscopy (FE-SEM) image of the NF
18 electrode after the hydrothermal deposition, which displays that the entire surface of the NF was
19 uniformly covered with NiCo₂O₄ composites without blocking or modifying the open
20 macroscopic porous structure of the NF.³⁸ The high-magnification FE-SEM images show the
21 vertically aligned NiCo₂O₄ nanowires with sharpened tips grown perpendicularly on the NF
22 (Figures 1b and S3a). These nanowire arrays were ~ 3.8 μm in length and ~ 150 nm in diameter
23 and were well separated from each other having its own direct contact with the NF at the bottom
24 (Figure S3b). Another important feature for excellent catalytic activity is the long-lasting
25 adherence of nanowire arrays to NF, which is beneficial for efficient electron transfer between
26 nanowire arrays and NF, resulting in an effective involvement of the nanowire arrays in redox
27 reactions.³⁹ The transmission electron microscopy (TEM) image in Figure S3c further shows that
28 the NiCo₂O₄ nanowire was built up by a number of nanoparticles that were stacked along one
29 direction predominantly in a rhombus and hexagonal shapes (marked by the respective shapes)
30 and distributed all over the nanowires.⁴⁰ It is worth noting that, these rhombus/hexagonal
31 nanoplates were interconnected with each other with no evidence of ruptures and lattice changes
32 at the edges. The high-resolution TEM (HR-TEM) image in Figure S3d reveals that the
33
34
35
36
37
38
39
40
41
42
43
44
45
46
47
48
49
50
51
52
53
54
55
56
57
58
59
60

nanoparticles were highly crystalline with a well-resolved lattice fringes of 0.278 ± 0.02 nm, which could be attributed to the (220) plane of spinel NiCo_2O_4 with the cubic phase.

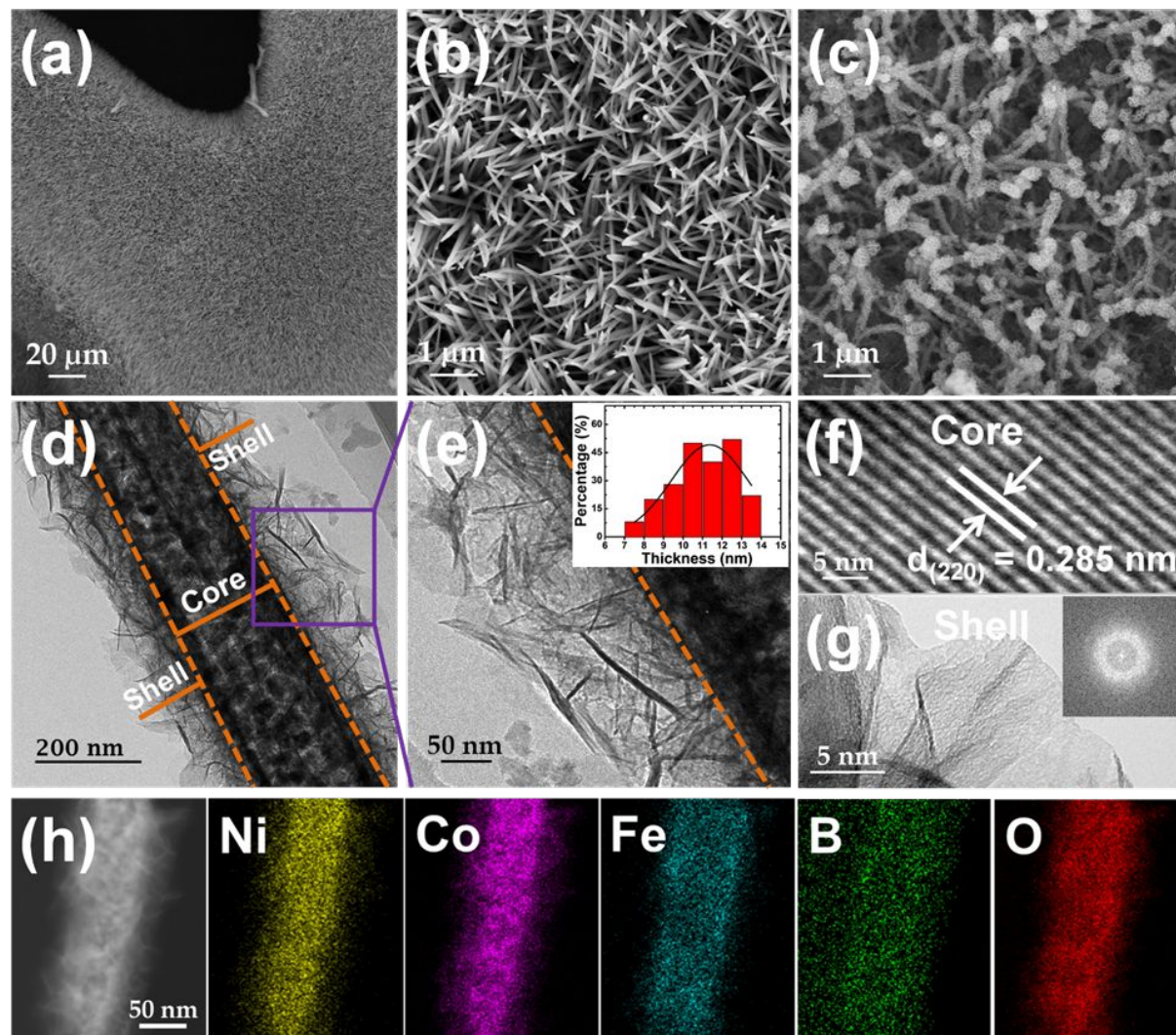


Figure 1. (a) Low and (b) high magnification FE-SEM images of the hydrothermally grown NiCo_2O_4 nanowires on NF ($\text{NiCo}_2\text{O}_4/\text{NF}$). (c) FE-SEM and (d) TEM images of the core-shell nanostructure of the $\text{Co-Fe-B}_i/\text{NiCo}_2\text{O}_4$. (e) Detailed image from the squared part in (d) depicting the closer view of the Co-Fe-B_i nanosheets. Inset shows the histogram for the thickness analysis of the Co-Fe-B_i nanosheets. (f) and (g) HR-TEM images of the NiCo_2O_4 nanowires and Co-Fe-B_i nanosheets, respectively. Inset of (g) shows the fast Fourier transform (FFT) pattern of

1
2
3 the Co-Fe-B_i nanosheets. (h) STEM image of the Co-Fe-B_i/NiCo₂O₄ and its corresponding EDS
4
5 elemental mapping images.
6
7

8
9 The hydrothermally grown 1D NiCo₂O₄ nanowires acted as a secondary platform for further
10
11 solution processing of the few layers of the 2D Co-Fe-B_i nanosheets, which created a synergy of
12
13 the Co and Fe bimetals and provided the benefits of the metal-metalloid structure for catalyzing
14
15 the OER efficiently. The facile solution processing facilitated uniform and vertical growth of the
16
17 Co-Fe-B_i nanosheets on the NiCo₂O₄ nanowires, leading to a typical 3D core-shell nanohybrid
18
19 structure (Figure 1c). We further deposited Co-Fe-B_i nanosheets on NF, which resulted in
20
21 ultrathin layers with thickness of several nanometers that appeared to be interconnected with
22
23 each other, creating a loose porous structure with a large open space and electrochemically active
24
25 surface area (Figure S4a and b).^{34,41,42} Additional low- and high-magnification FE-SEM images
26
27 of the 3D core-shell nanohybrids in Figure S5 depict the unique mesoporous structure composed
28
29 of a few layers of Co-Fe-B_i nanosheets uniformly covering the NiCo₂O₄ nanowire arrays. We
30
31 expected that an attractive 3D core-shell nanohybrid electrocatalyst would accelerate the
32
33 electrolyte penetration and ion diffusion within the electrode for rapid redox reactions, thereby
34
35 increasing the electrocatalytic performance towards the OER.^{31,43} The role of these unique 3D
36
37 core-shell nanohybrid structure in increasing the electrochemical performance has been
38
39 confirmed by previous reports as well.^{31,38,40,41} The energy-dispersive X-ray spectrum (EDS)
40
41 clearly revealed the presence of Ni, Co, Fe, O and B elements in the 3D core-shell nanohybrid
42
43 (Figure S6). The TEM image in Figure 1d further demonstrates that the diameter of the 3D core-
44
45 shell nanohybrid was ~ 320 nm, in which an outer shell of Co-Fe-B_i nanosheets (~ 170 nm) were
46
47 vertically grafted onto the inner core NiCo₂O₄ nanowires (~ 150 nm) without altering the
48
49 uniform nanowire array structure. Unlike the usual core-shell nanostructure, the outer shell of the
50
51
52
53
54
55
56
57
58
59
60

1
2
3 Co-Fe-B_i nanosheets crosslinked to the inner NiCo₂O₄ nanowire core, creating many void spaces
4 between the nanosheets (Figures S4 and S5), and thus allowed easy access of the inner NiCo₂O₄
5 core to the electrolyte.⁴⁴ Figure 1e is the closer view of the Co-Fe-B_i nanosheets, in which the
6 edges of the nanosheets are almost transparent due to the ultrathin nature of the nanosheets.
7
8 Furthermore, the statistical analysis revealed the thickness of each Co-Fe-B_i nanosheet to be ~ 10
9 to 12 nm (Figure 1e, inset), indicating the few layers characteristic in the 3D core-shell
10 nanohybrids. Moreover, in the HR-TEM images (Figure 1f and g), the interplanar spacing of the
11 well-resolved lattice fringes in the core is $\sim 0.285 \pm 0.02$ nm, which is indexed to the (220) plane
12 of the spinel structured NiCo₂O₄ (JCPDS: 73-1702), while the shell edge shows the amorphous
13 nature, further confirmed by the fast Fourier transform (FFT) pattern (Figure 1g, inset). Note that
14 the amorphous electrocatalysts had abundant unsaturated active sites, leading to a higher OER
15 activity compared to that of their crystalline counterparts.^{33,45} Additionally, scanning TEM
16 (STEM) and the corresponding EDS elemental mapping images (Figure 1h) reveal the
17 quintessential core-shell structure with a uniform and homogenous distribution of Ni, Co, Fe, B,
18 and O elements throughout the whole structure without aggregation or segregations.

19
20
21
22
23
24
25
26
27
28
29
30
31
32
33
34
35
36
37
38 X-ray diffraction (XRD) measurements were carried out to further investigate the phases of the
39 samples. In the XRD pattern of the Co-Fe-B_i/NiCo₂O₄/NF electrode (Figure 2a), all the peaks
40 were indexed to the spinel NiCo₂O₄ in the cubic structure (JCPDS: 73-1702), except for the
41 strong diffraction peaks of the Ni substrate (marked by '#'). The Co-Fe-B_i nanosheets displayed
42 an amorphous nature, which was also confirmed by the XRD and TEM images of the pure Co-
43 Fe-B_i/NF (Figure 1g and S7). X-ray photoelectron spectroscopy (XPS) was employed to
44 elucidate the chemical composition and oxidation state of the elements. The XPS survey
45 spectrum, as shown in Figure S8a, revealed the presence of Ni, Co, and O elements in the
46
47
48
49
50
51
52
53
54
55
56
57
58
59
60

1
2
3 NiCo₂O₄/NF. The core-level Ni 2p XPS spectrum (Figure S8b) showed two peaks at 854.38 eV
4 and 871.5 eV corresponding to Ni 2p_{3/2} and Ni 2p_{1/2}, respectively.⁴⁶ The core-level Co 2p XPS
5 spectrum showed that the Co atoms were in the Co 2p_{3/2} and Co 2p_{1/2} electronic configurations,
6 with peaks located at 778.5 eV and 793.8 eV (Figure S8c), suggesting that the Co was present in
7 the Co²⁺ and Co³⁺ states. These results further confirmed the formation of NiCo₂O₄ in the cubic
8 phase.⁴⁷ As displayed in Figure S9 in the XPS survey spectrum of the Co-Fe-B_i/NiCo₂O₄/NF, all
9 the elements of Ni, Co, Fe, B and O were present in the core-shell nanohybrid. Figure 2b and c
10 depict the high-resolution core-level spectra of Co 2p and Fe 2p, respectively. The peaks located
11 at 780.9 eV and 797.1 eV accompanied by the satellite peaks were ascribed to the Co 2p_{3/2} and
12 Co 2p_{1/2}, respectively, which are the characteristic binding energies of Co²⁺.⁴⁸ In addition, the
13 core-level Fe 2p spectrum (Figure 2c) can be fitted into Fe 2p_{3/2} (711.9 eV) and Fe 2p_{1/2} (725.1
14 eV) accompanied by two satellite peaks, indicating that the Fe was in the Fe³⁺ oxidation state.⁴⁸
15 When these Fe³⁺ species combines with Co species, the electronic structure and conductivity
16 improves, which drastically promotes the OER ability.^{24, 25, 49} Also, Xiao et al. reported the
17 synergistic effect between Co and Fe towards the enhanced OER activity in Fe-doped Co₃O₄.⁵⁰
18 In addition, Burke et al. reported the existence of strong electronic interactions between Co and
19 Fe element and found that the Fe plays an crucial role for enhanced OER activity.⁵¹
20
21
22
23
24
25
26
27
28
29
30
31
32
33
34
35
36
37
38
39
40
41

42 The high-resolution B 1s spectrum (Figure 2d) showed one clear peak at ~ 192.4 eV, which
43 was assigned to the B-O bonding in the borate.⁵² The high-resolution O 1s spectra (Figures 2e
44 and S8d) was fitted into three oxygen species. Specifically, the binding energy peak at 529.7 eV
45 can be ascribed to the oxygen-metal (O 1s A); the peak located at 531.5 eV is usually associated
46 with the oxygen from hydroxyl groups (O 1s B), and the peak at 533.1 eV is attributed to the
47 surface adsorbed H₂O molecule (O 1s C). Moreover, after the hybridization, as shown in the O
48
49
50
51
52
53
54
55
56
57
58
59
60

1s core level spectra in Figure 2e, the overall intensity of the XPS spectrum was significantly decreased, whereas the O 1s A peak became more predominant. This could be attributed to the strong B-O bonds after the deposition of the Co-Fe-B_i nanosheets on the NiCo₂O₄ nanowires. Moreover, the O 1s spectrum of the Co-Fe-B_i/NiCo₂O₄/NF electrode was shifted towards the negative binding energy, indicating the strong electronic interactions and chemical coupling at the interface between the Co-Fe-B_i nanosheets and NiCo₂O₄ nanowires,³⁸ making it a legitimate candidate as an electrocatalyst for water oxidation.

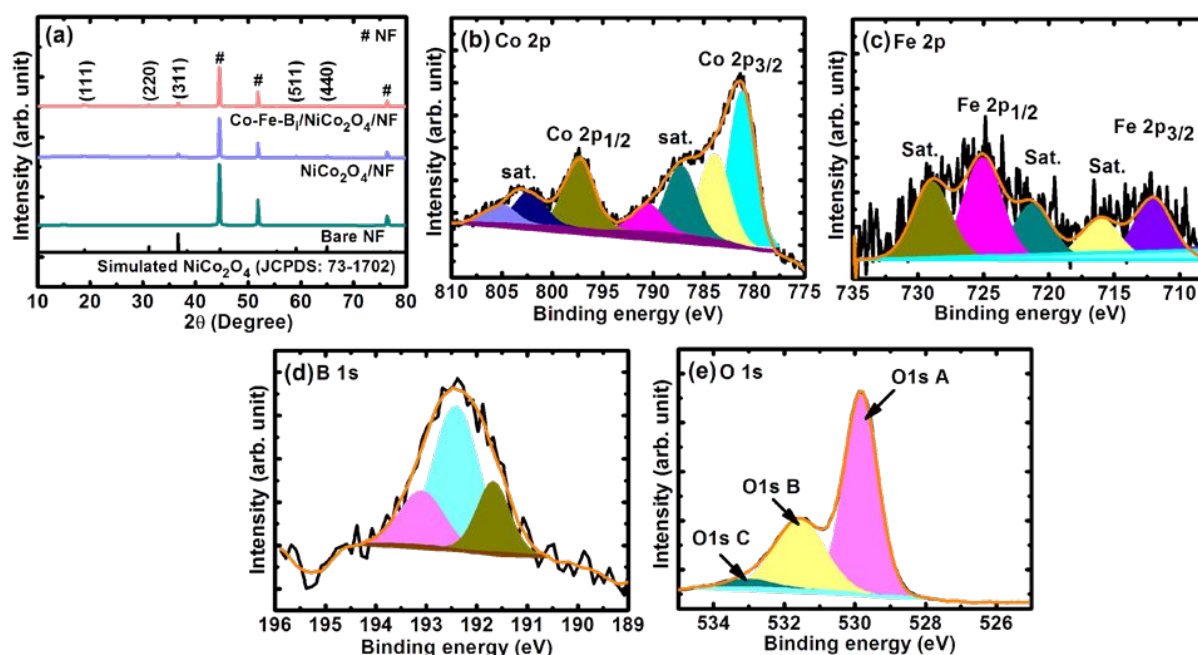


Figure 2. (a) XRD patterns of the bare NF, NiCo₂O₄/NF, Co-Fe-B_i/NiCo₂O₄/NF electrodes. The peaks marked by ‘#’ are associated with the NF. High-resolution core-level spectra of (b) Co 2p, (c) Fe 2p, (d) B 1s (e) O 1s of Co-Fe-B_i/NiCo₂O₄/NF.

The electrocatalytic OER performance of the self-standing 3D core-shell Co-Fe-B_i/NiCo₂O₄/NF nanohybrid electrode, along with that of the pure Co-Fe-B_i/NF, NiCo₂O₄/NF and RuO₂/NF, was evaluated in 1 M aqueous KOH electrolyte using a conventional three-electrode

1
2
3 electrochemical system. The as-prepared 3D core-shell nanohybrid structure grown on the NF
4 was directly used as a self-standing, binder-free electrode for evaluating the electrocatalytic OER
5 performance. To achieve stability and reversibility, the as-prepared electrodes were initially
6 treated with several continuous electrochemical conditioning cycles (Figure S10) prior to the
7 collection of linear sweep voltammetry curves. As shown in the polarization curves and
8 comparison plot (Figure 3a and b), the Co-Fe-B_i/NiCo₂O₄/NF nanohybrid only required an
9 overpotential of 227 mV to achieve a current density of 10 mA/cm², which was significantly
10 lower than that of the Co-Fe-B_i/NF (321 mV), NiCo₂O₄/NF (345 mV), and RuO₂/NF (382 mV)
11 and many other reported OER electrocatalysts (Table S1). However, it is slightly higher (~ 50
12 mV) than the best-ever reported overpotential of 177 mV at 10 mA/cm² using Fe(PO₃)₂/Ni₂P
13 electrocatalysts for OER by Ren et al.⁵³ Surprisingly, the Co-Fe-B_i/NiCo₂O₄/NF nanohybrid
14 electrocatalyst delivered a current density of 200 mA/cm², close to the industrial current density
15 of water electrolysis at the required overpotential of ~ 410 mV, which was obviously less than
16 that of the Co-Fe-B_i/NF (585 mV), NiCo₂O₄/NF (647 mV), and RuO₂/NF (678 mV)
17 electrocatalysts. The achieved OER performance was solely attributed to the 3D core-shell
18 nanohybrid structure, which provided strong chemical coupling, efficient electrolyte diffusion
19 and bubble detachment, abundant active sites for the OER and rapid charge transfer between the
20 interfaces.⁴⁴ The superior electrocatalytic performance was further assessed by the Tafel plots,
21 and more promising OER kinetics and superior catalytic activity were indicated by the low Tafel
22 slope.⁵⁴ As shown in Figure 3c, the Co-Fe-B_i/NiCo₂O₄/NF nanohybrid electrode showed the
23 smallest Tafel slope of 45 mV dec⁻¹ compared to those of the Co-Fe-B_i/NF (71.4 mV dec⁻¹),
24 NiCo₂O₄/NF (80.1 mV dec⁻¹) and RuO₂/NF (96.3 mV dec⁻¹), respectively, indicating that the
25 nanohybrid electrocatalyst expedited the OER kinetics. The favorable OER kinetics was
26
27
28
29
30
31
32
33
34
35
36
37
38
39
40
41
42
43
44
45
46
47
48
49
50
51
52
53
54
55
56
57
58
59
60

1
2
3 supposed to be originated from the numerous active sites created by the 3D core-shell
4 nano hybrid structure and the intrinsic catalytic activities of the strongly coupled Co-Fe-B_i
5 nanosheets and NiCo₂O₄ nanowires. In light of the high OER activity, long-term durability is an
6 important aspect in determining the quality of the electrocatalysts. The Co-Fe-B_i/NiCo₂O₄/NF
7 core/shell nano hybrid electrocatalyst retained about 96% of the initial current density after the
8 stability test for 40 h, revealing its long-term durability (Figure 3d). To further elucidate the
9 electrode/electrolyte interface behavior and reaction kinetics, an electrochemical impedance
10 spectroscopy (EIS) measurements was carried out (Figure 3e), and the corresponding data were
11 fitted with the Randles equivalent circuit (Figure S11). The resistance in the high frequency
12 region of the Nyquist plots was associated with the uncompensated solution resistance (R_s), and
13 all the electrocatalysts were found to exhibit similar R_s values as the measurements were carried
14 out in the same cell with the same counter-electrode and inter-electrode gap. Furthermore, the
15 charge transfer resistance (R_{ct}) was evaluated to determine the OER reaction kinetics from the
16 middle and low frequency regions of the Nyquist plots, in which a smaller R_{ct} reflects faster
17 reaction kinetics.⁵⁵ The 3D core-shell Co-Fe-B_i/NiCo₂O₄/NF nano hybrid electrocatalyst
18 exhibited an R_{ct} as low as 26.3 Ω , which was smaller than that of the Co-Fe-B_i/NF (54.9 Ω) and
19 NiCo₂O₄/NF (36.1 Ω). The strong coupling of the active Co-Fe-B_i nanosheets on the conducting
20 NiCo₂O₄ nanowires to form the 3D core-shell nano hybrid may have lowered the R_{ct} , and thus
21 favor the rapid-charge transfer that resulted in the remarkable OER activity of the Co-Fe-
22 B_i/NiCo₂O₄/NF nano hybrid electrocatalyst.²⁷
23
24
25
26
27
28
29
30
31
32
33
34
35
36
37
38
39
40
41
42
43
44
45
46
47
48
49
50
51
52
53
54
55
56
57
58
59
60

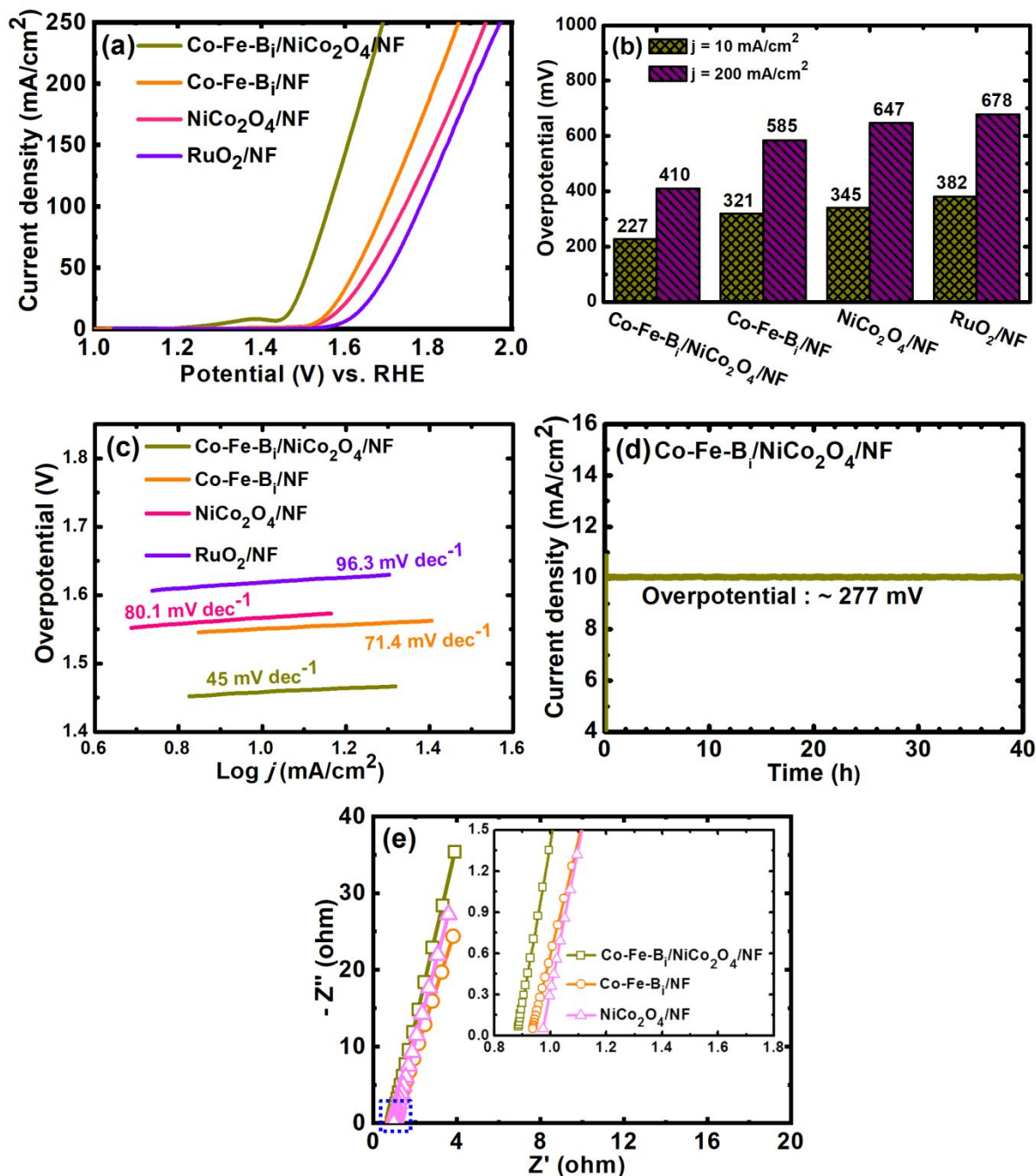


Figure 3. (a) OER Polarization curves, (b) overpotential comparison plots, and (c) corresponding Tafel plots of the Co-Fe-B_i/NiCo₂O₄/NF, Co-Fe-B_i/NF, NiCo₂O₄/NF, and RuO₂/NF electrocatalysts. (d) Long-term durability test of the Co-Fe-B_i/NiCo₂O₄/NF at a constant overpotential of ~ 227 mV for 40 h. (e) Nyquist plots for the Co-Fe-B_i/NiCo₂O₄/NF, Co-Fe-

1
2
3 B_i/NF , and $NiCo_2O_4/NF$ electrocatalysts. The inset in (e) shows the enlarged EIS curves of the
4
5 blue squared part. All the electrochemical measurements were carried out in 1 M KOH
6
7 electrolyte (pH = 14) at 10 mV s^{-1} .
8
9

10
11 The cyclic voltammetry (CV) measurements in non-Faradaic region were carried out to
12
13 determine the double-layer capacitance (C_{dl}), which is proportional to the electrochemically
14
15 active surface area (ECSA), which sheds a light on the possible origins of the outstanding OER
16
17 activity of the Co-Fe- $B_i/NiCo_2O_4/NF$ nanohybrid electrocatalyst.⁵⁶ Figure 4a shows the
18
19 capacitive currents as a function of the scan rate obtained from the corresponding CV curves to
20
21 calculate C_{dl} for the all the electrocatalysts (Figure S12 and Table S2). The C_{dl} of Co-Fe-
22
23 $B_i/NiCo_2O_4/NF$ nanohybrid electrocatalyst was ~ 2.5 and ~ 3.3 times larger than those of the Co-
24
25 Fe- B_i/NF and $NiCo_2O_4/NF$, respectively, demonstrating that the 3D core-shell nanohybrid
26
27 structure with larger ECSA exposed the numerous catalytically active sites for water
28
29 electrolysis.²⁶ It has been speculated that the large ECSA allows close contact with the
30
31 electrolyte and easy adsorption of water molecules and provides abundant active sites for
32
33 catalytic reactions, which obviously accounts for the improved OER activity.^{26,44} The
34
35 investigation of porous nature and the specific active surface area of Co-Fe- $B_i/NiCo_2O_4/NF$, Co-
36
37 Fe- B_i/NF , and $NiCo_2O_4/NF$ using the Brunauer-Emmett-Teller (BET) measurements (Figure 4b
38
39 and S13). The Co-Fe- $B_i/NiCo_2O_4/NF$ nanohybrid electrocatalyst exhibits an active surface area
40
41 of $\sim 16.8\text{ m}^2/\text{g}$, significantly higher than that of the Co-Fe- B_i/NF ($11.9\text{ m}^2/\text{g}$) and $NiCo_2O_4/NF$
42
43 ($1.6\text{ m}^2/\text{g}$) electrocatalysts, exposing more actives and large contact area for catalysis.
44
45
46
47
48
49
50
51
52
53
54
55
56
57
58
59
60

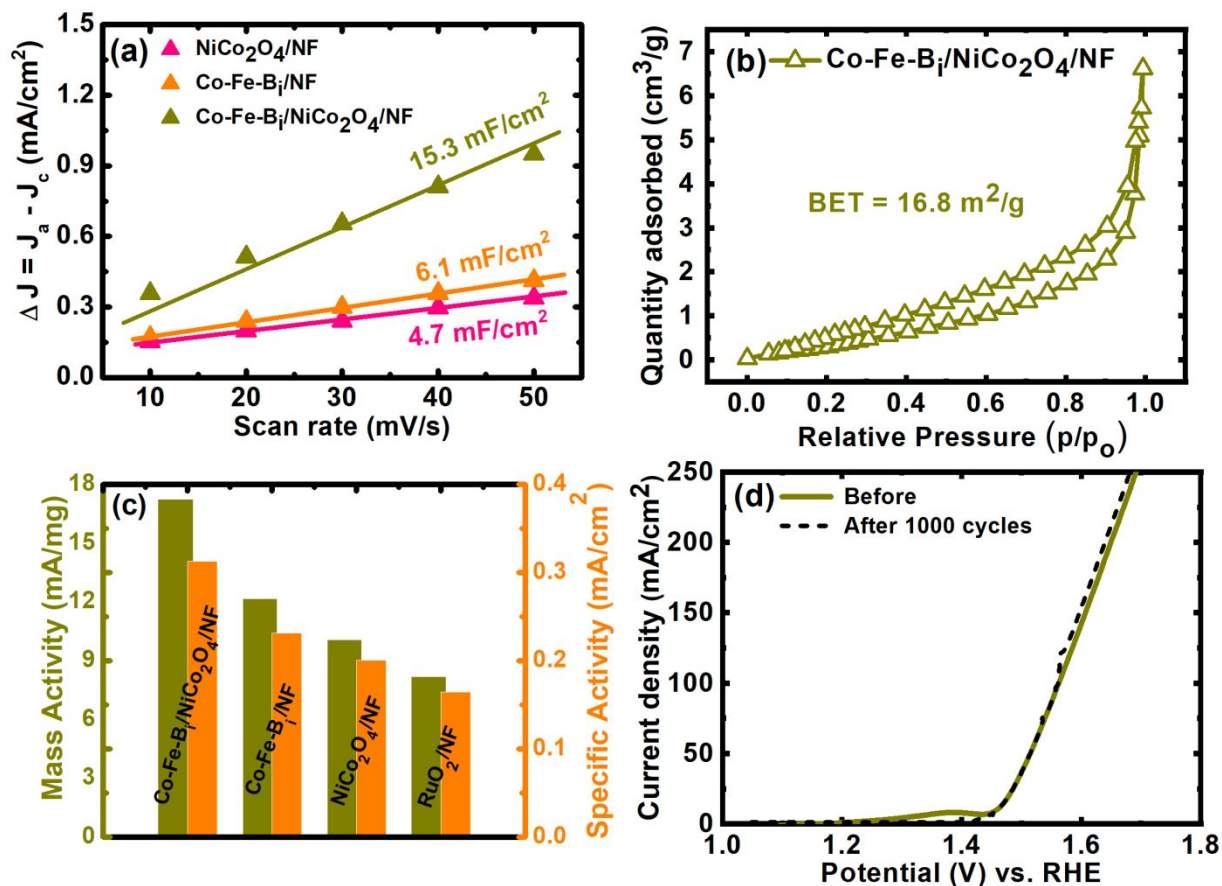


Figure 4. (a) Capacitive currents as a function of scan rate plots obtained from the CV curves of the different electrocatalysts. (b) N₂ desorption isotherm of the Co-Fe-B_i/NiCo₂O₄/NF used to evaluate the BET-specific active surface area. (c) Estimated mass activity (MA) and specific activity (SA) of the different electrocatalysts. (d) OER polarization curves recorded for the Co-Fe-B_i/NiCo₂O₄/NF before and after 1000 CV scanning cycles.

To further evaluate the intrinsic OER activity of the electrocatalysts, the mass activity (MA) (normalized to the mass loading) and specific activity (SA) (normalized to the surface area from BET measurements) were estimated and are presented in Figure 4c. The Co-Fe-B_i/NiCo₂O₄/NF nanohybrid electrocatalyst exhibited a mass activity of 17.2 mA mg⁻¹, which was ~ 1.4 and ~ 1.7 times higher than that of the Co-Fe-B_i/NF and NiCo₂O₄/NF electrocatalysts, respectively. It has been suggested that the intrinsic activity of the electrocatalysts is well reflected by the specific

activity.⁵⁷ Thus, further evaluation of the specific activity disclosed that the intrinsic OER activity of the electrocatalysts followed the order of Co-Fe-B_i/NiCo₂O₄/NF > Co-Fe-B_i/NF > NiCo₂O₄/NF > RuO₂/NF, again confirming the superior OER activity of the Co-Fe-B_i/NiCo₂O₄/NF nano hybrid electrocatalyst. Moreover, the continuous linear sweep voltammetric (LSV) scanning for 1000 cycles exhibited a negligible difference in oxygen evolution, further evidencing the excellent electrochemical stability (Figure 4d). We assumed that the continuous OER process promoted the in-situ transformation of the Co-Fe-B_i shell into Co-Fe-based hydroxides, which have been demonstrated to be active sites for the OER.⁵⁸

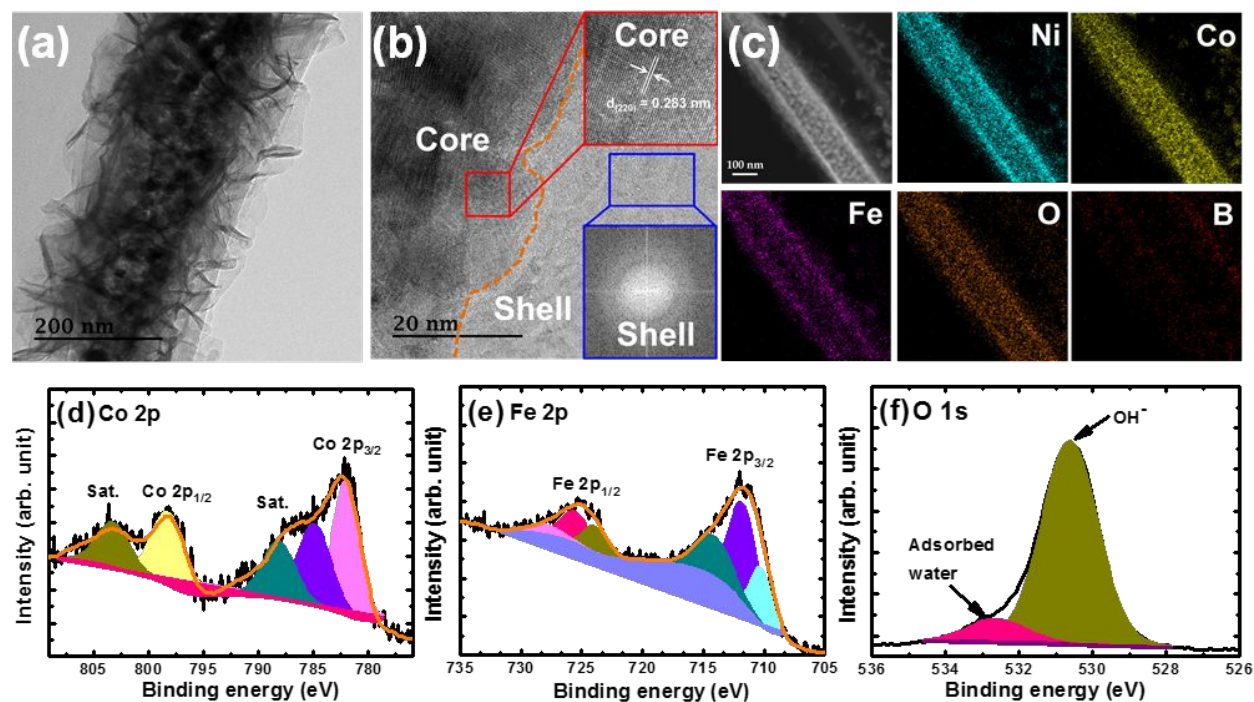


Figure 5. Characterizations after the durability test. (a) TEM, (b) HR-TEM, and (c) STEM and EDS elemental mapping images of Co-Fe-B_i/NiCo₂O₄/NF electrocatalyst after the durability test for 40 h. High-resolution core-level spectra of (d) Co 2p (e) Fe 2p, and (f) O 1s of after the durability test for 40 h.

1
2
3 To verify the above hypothesis, we further examined the morphology and composition of the
4 Co-Fe-B_i/NiCo₂O₄/NF nanohybrid electrocatalyst after a durability test for 40 h. Figure S14a
5 shows the FE-SEM image of the Co-Fe-B_i/NiCo₂O₄/NF nanohybrid after the OER durability test,
6 which indicated that the electrocatalyst retained the 3D core-shell nanohybrid structure. The
7 TEM image in Figure 5a clearly reveals the well-preserved core-shell nanohybrid structure of the
8 nanosheet shell and the NiCo₂O₄ nanowire core even after the prolonged durability test for 40 h.
9 Notably, the interplanar spacing of $\sim 0.283 \pm 0.02$ nm, which is indexed to the (220) plane of the
10 spinel structured NiCo₂O₄ (JCPDS: 73-1702) core, along with the amorphous shell, was still
11 observed after the OER test (Figure 5b). Interestingly, the STEM and EDS elemental mapping
12 images in Figure 5c further confirm the intact core-shell nanohybrid structure with a
13 homogenous distribution of all the elements except for B elements.
14
15
16
17
18
19
20
21
22
23
24
25
26
27

28 The inductively coupled plasma mass spectrometry (ICP-MS) analysis further revealed the loss
29 of B and increase of O species after the OER test. Specifically, the atomic ratio for B decreased
30 from $\sim 24\%$ in the pristine Co-Fe-B_i sample to $\sim 1\%$ in the post-OER sample, whereas the
31 atomic ratio of O increased from 38% for the pristine sample to 62% for the post-OER sample.
32 These findings were further confirmed by the XPS analysis (Figures 5d-f and S14b). In the high-
33 resolution spectra of the Co 2p, Fe 2p, B 1s and O 1s spin-orbitals, all the peaks associated with
34 the borate species almost entirely disappeared after the OER test. The core-level XPS spectrum
35 of Co 2p after the OER showed peaks at 781.6 eV and 796.4 eV for the Co 2p_{1/2} and Co 2p_{3/2}
36 energy levels along with the presence of weak satellite peaks at 802.6 eV, 784.3 eV and 788.2
37 eV, respectively, suggesting the transformation of Co from +2 to the higher oxidation state of +3
38 (CoOOH phase) during the OER process (Figure 5d). This transformation can also be confirmed
39 from the anodic peak at ~ 1.38 V vs RHE in Figure 4(d), which was later disappeared after
40
41
42
43
44
45
46
47
48
49
50
51
52
53
54
55
56
57
58
59
60

1
2
3 continuous OER process, suggesting the complete transformation of Co-Fe-B_i to Co-Fe-OOH.
4
5 However, no change in the Fe 2p spectrum was observed after the OER test, indicating the
6
7 valence state of Fe was +3 (Figure 5e). Interestingly, the O 1s spectrum showed the absence of
8
9 the B-O bond and the evolution of a new peak at ~ 531.6 eV, suggesting that the O coordination
10
11 environment changed after the OER test. Similarly, the B 1s spectrum (Figure S14b) confirmed
12
13 the absence of a peak corresponding to the B-O bond, suggesting the B species were almost
14
15 completely transferred to the electrolyte, which was consistent with the EDS elemental mapping
16
17 results (Figure 5c). These observations from the morphological and compositional
18
19 characterizations indicated that the Co-Fe-B_i shell oxidized to Co-Fe-OOH during the OER test,
20
21 which are considered to be active sites for efficient water oxidation.^{57, 58}
22
23
24
25

26 Finally, the excellent catalytic activity and durability of the Co-Fe-B_i/NiCo₂O₄/NF nanohybrid
27
28 electrocatalyst can be attributed to the following factors: (I) The facile growth of the Co-Fe-B_i
29
30 nanosheets and NiCo₂O₄ nanowires on the highly conductive 3D NF porous structure enabled
31
32 close contact and strong adhesion in the nanohybrid structure. Thus, the intrinsic assets and
33
34 robust coupling effects of the 3D core-shell nanohybrid structure contributed to the high activity
35
36 and durability towards water oxidation. (II) The direct grafting of the Co-Fe-B_i nanosheets on the
37
38 NiCo₂O₄ nanowires grown on the NF ensured efficient charge transport by allowing more
39
40 effective shuttling of the charges at the heterostructure interfaces, as confirmed by the lower R_{ct}
41
42 obtained from the EIS analysis (Figure 3e). (III) The unique 3D core-shell nanohybrid structure
43
44 of the Co-Fe-B_i nanosheet shell and NiCo₂O₄ nanowire core on the free-standing NF current
45
46 collector provided an excellent pathway for both ion and electrolyte diffusion, and it was
47
48 beneficial for the instantaneous release of O₂ bubbles. (IV) Last, the excellent OER
49
50 performances of the core-shell nanohybrid structure can also be partially ascribed to the possible
51
52
53
54
55
56
57
58
59
60

1
2
3 formation of an amorphous Co-Fe-OOH, which has been proved to promote the exposure of
4 more active sites during the OER.^{57, 58} Synergistically, these advantages endowed the self-
5 standing 3D core-shell Co-Fe-B_i/NiCo₂O₄/NF nanohybrid electrocatalyst with remarkable
6 catalytic activity and durability towards water oxidation.
7
8
9
10
11

12 CONCLUSION

13
14 In conclusion, we demonstrated an advanced self-standing 3D core-shell nanohybrid structure
15 composed of an ultrathin Co-Fe-B_i nanosheet shell and a NiCo₂O₄ nanowire core on a self-
16 standing NF support through a two-step facile method for highly efficient and durable water
17 oxidation. This unique 3D nanohybrid structure provides the following characteristics for
18 efficient water oxidation: (1) amorphous Co-Fe-B_i nanosheets and crystalline NiCo₂O₄
19 synergistically create strong interactions, which obviously promote the reaction kinetics to speed
20 up the water oxidation; (2) electrocatalysts with a 3D core-shell nanohybrid structure with high
21 specific surface area and abundant active sites offer fast transport behavior of electrolytes and
22 gases, which is beneficial for water oxidation; and (3) an advanced 3D self-supported electrode
23 configuration with macropore channels allows for harnessing the effective penetration of
24 electrolytes, and thus guarantees a durable lifespan towards efficient water oxidation. As a result,
25 the Co-Fe-B_i/NiCo₂O₄/NF nanohybrid electrocatalyst exhibits one of the best electrocatalytic
26 OER performances among the reported borate-based electrocatalysts and is comparable to most
27 of the noble-metal-free electrocatalysts. Our work opens new pathways for the rational design
28 and development of the advanced nanomaterials with exciting electronic properties and surface
29 structures for a multitude of renewable energy-related and other catalytic applications.
30
31
32
33
34
35
36
37
38
39
40
41
42
43
44
45
46
47
48
49
50
51
52
53
54
55
56
57
58
59
60

ASSOCIATED CONTENT

Supporting Information. Experimental section, characterizations techniques, and electrochemical measurements, additional figures such as photographs of bare NF and different electrocatalysts, additional FE-SEM and TEM images of different electrocatalysts, EDS spectrum of Co-Fe-B_i/NiCo₂O₄/NF electrocatalyst, XRD patterns of Co-Fe-B_i powder and Co-Fe-B_i grown on NF and TEM image of Co-Fe-B_i, survey and core-level XPS spectra of NiCo₂O₄/NF electrocatalyst, survey spectrum of Co-Fe-B_i/NiCo₂O₄/NF, continuous CV cycling plots of different electrocatalysts, Randles equivalent circuit model used to stimulate the Nyquist plots from EIS measurements, CV curves measured at different scan rates for different electrocatalysts, N₂ absorption-desorption isotherm of Co-Fe-B_i/NF, and NiCo₂O₄/NF, of Fe-SEM image and core-level XPS spectrum of B 1s of Co-Fe-B_i/NiCo₂O₄/NF electrocatalysts after stability test, and Tables representing the comparison of OER performance for Co-Fe-B_i/NiCo₂O₄/NF with other non-noble-metals-based borates and other electrocatalysts and estimated R_s and R_{ct} values of different electrocatalysts by fitting the EIS spectra using ZView software.

AUTHOR INFORMATION

Corresponding Authors

*Jin Hyeok Kim, Email: jinhyeok@chonaam.ac.kr

*Seung Wook Shin, Email: swshin1211@gmail.com

*Mahesh P. Suryawanshi, Email: m.suryawanshi@unsw.edu.au

ORCID

Umesh P. Suryawanshi: 0000-0002-1657-2519

Mahesh P. Suryawanshi: 0000-0003-4711-7655

1
2
3 Uma V. Ghorpade: 0000-0001-8631-7030x
4

5 Seung Wook Shin: 0000-0003-1401-6145
6

7 Jin Hyeok Kim: 0000-0002-2220-1941
8
9

10 11 12 **Author Contributions** 13

14 ‡U. P. S. and M. P. S contributed equally to this work. J. H. K., S. W. S. and M. P. S. conceived
15 and supervised the research. U. P. S. and M. P. S. designed and performed most of the
16 experiments and data analysis and wrote the manuscript. U. V. G., M. H., and D. L. participated
17 in various aspects of the discussions during the preparation of the manuscript. All authors have
18 given approval to the final version of the manuscript.
19
20
21
22
23
24
25
26
27

28 29 **ACKNOWLEDGMENT** 30

31 This work was supported by the Human Resources Development Program (No.
32 20194030202470) of the Korea Institute of Energy Technology Evaluation and Planning
33 (KETEP) funded by the Korea Government Ministry of Trade, Industry and Energy and was
34 partially supported by the Priority Research Centers Program through the National Research
35 Foundation of Korea (NRF) funded by the Ministry of Education, Science and Technology
36 (2018R1A6A1A03024334).
37
38
39
40
41
42
43
44
45
46

47 48 **REFERENCES** 49

50 (1) Zhu, X.; Tang, C.; Wang, H.-F.; Li, B.-Q.; Zhang, Q.; Li, C.; Yang, C.; Wei, F. Monolithic-
51 structured ternary hydroxides as freestanding bifunctional electrocatalysts for overall water
52 splitting, *J. Mater. Chem. A* **2016**, *4*, 7245–7250.
53
54
55
56
57
58
59
60

- 1
2
3 (2) Kumar, A.; Bhattacharyya, S. Porous NiFe-Oxide Nanocubes as Bifunctional Electrocatalysts
4 for Efficient Water-Splitting, *ACS Appl. Mater. Interfaces* **2017**, *9*, 41906–41915.
5
6
7 (3) Zhou, W.; Wu, X. -J.; Cao, X.; Huang, X.; Tan, C.; Tian, J.; Liu, H.; Wang, J.; Zhang, H.
8 Ni₃S₂ nanorods/Ni foam composite electrode with low overpotential for electrocatalytic oxygen
9 evolution, *Energy Environ. Sci.* **2013**, *6*, 2921–2924.
10
11
12 (4) Bediako, D. K.; Surendranath, Y.; Nocera, D. G. Mechanistic Studies of the Oxygen
13 Evolution Reaction Mediated by a Nickel–Borate Thin Film Electrocatalyst, *J. Am. Chem. Soc.*
14 **2013**, *135*, 3662–3674.
15
16
17 (5) Suntivich, J.; May, K. J.; Gasteiger, H. A.; Goodenough, J. B.; Shao-Horn, Y. A Perovskite
18 Oxide Optimized for Oxygen Evolution Catalysis from Molecular Orbital Principles, *Science*
19 **2011**, *334*, 1383–1385.
20
21
22 (6) Wang, H.; Lee, H. W.; Deng, Y.; Lu, Z.; Hsu, P.C.; Liu, Y.; Lin, D.; Cui, Y. Bifunctional
23 non-noble metal oxide nanoparticle electrocatalysts through lithium-induced conversion for
24 overall water splitting, *Nat. Commun.* **2015**, *6*, 7261.
25
26
27 (7) McCrory, C. C.; Jung, S.; Ferrer, I. M.; Chatman, S. M.; Peters, J. C.; Jaramillo, T. F.
28 Benchmarking Hydrogen Evolving Reaction and Oxygen Evolving Reaction Electrocatalysts for
29 Solar Water Splitting Devices, *J. Am. Chem. Soc.* **2015**, *137*, 4347–4357.
30
31
32 (8) Das, R. K.; Wang, Y.; Vasilyeva, S. V.; Donoghue, E.; Pucher, I.; Kamenov, G.; Cheng, H.
33 P.; Rinzler, A. G. Extraordinary Hydrogen Evolution and Oxidation Reaction Activity from
34 Carbon Nanotubes and Graphitic Carbons, *ACS Nano* **2014**, *8*, 8447–8456.
35
36
37 (9) Rosen, J.; Hutchings, G. S.; Jiao, F. Ordered Mesoporous Cobalt Oxide as Highly Efficient
38 Oxygen Evolution Catalyst, *J. Am. Chem. Soc.* **2013**, *135*, 4516–4521.
39
40
41
42
43
44
45
46
47
48
49
50
51
52
53
54
55
56
57
58
59
60

- 1
2
3 (10) Tian, J.; Liu, Q.; Asiri, A. M.; Sun, X. Self-Supported Nanoporous Cobalt Phosphide
4 Nanowire Arrays: An Efficient 3D Hydrogen-Evolving Cathode over the Wide Range of pH 0–
5 14, *J. Am. Chem. Soc.* **2014**, *136*, 7587–7590.
6
7
8
9
10 (11) Zhang, J.; Zhao, A.; Xia, Z.; Dai, L. A metal-free bifunctional electrocatalyst for oxygen
11 reduction and oxygen evolution reactions, *Nat. Nanotechnol.* **2015**, *10*, 444–452.
12
13
14 (12) Suryawanshi, M. P.; Ghorpade, U. V.; Shin, S. W.; Suryawanshi, U. P.; Shim, H. J.; Kang,
15 S. H.; Kim, J. H. Facile, Room Temperature, Electroless Deposited (Fe_{1-x},Mn_x)OOH Nanosheets
16 as Advanced Catalysts: The Role of Mn Incorporation, *Small* **2018**, *14*, e1801226.
17
18
19 (13) Liu, Y.; Cheng, H.; Lyu, M.; Fan, S.; Liu, Q.; Zhang, W.; Zhi, Y.; Wang, C.; Xiao, C.; Wei,
20 S.; Ye, B.; Xie, Y. Low Overpotential in Vacancy-Rich Ultrathin CoSe₂ Nanosheets for Water
21 Oxidation, *J. Am. Chem. Soc.* **2014**, *136*, 15670–15675.
22
23
24 (14) Zhu, Y. -P.; Liu, Y.-P.; Ren, T.-Z.; Yuan, Z.-Y. Self-Supported Cobalt Phosphide
25 Mesoporous Nanorod Arrays: A Flexible and Bifunctional Electrode for Highly Active
26 Electrochemical Water Reduction and Oxidation, *Adv. Funct. Mater.* **2015**, *25*, 7395.
27
28
29 (15) Gao, M. R.; Cao, X.; Gao, Q.; Xu, Y. F.; Zheng, Y. R.; Jiang, J.; Yu, S. H. Nitrogen-Doped
30 Graphene Supported CoSe₂ Nanobelt Composite Catalyst for Efficient Water Oxidation, *ACS*
31 *Nano* **2014**, *8*, 3970–3978.
32
33
34 (16) Zheng, Y. -R.; Gao, M. -R.; Gao, Q.; Li, H. -H.; Xu, J.; Wu, Z. -Y.; Yu, S. -H. An Efficient
35 CeO₂/CoSe₂ Nanobelt Composite for Electrochemical Water Oxidation, *Small* **2015**, *11*, 182–
36 188.
37
38
39 (17) Stern, L. -A.; Feng, L.; Song, F.; Hu, X. Ni₂P as a Janus catalyst for water splitting: the
40 oxygen evolution activity of Ni₂P nanoparticles, *Energy Environ. Sci.* **2015**, *8*, 2347–2351.
41
42
43
44
45
46
47
48
49
50
51
52
53
54
55
56
57
58
59
60

1
2
3 (18) Popczun, E. J.; McKone, J. R.; Read, C. G.; Biacchi, A. J.; Wiltrout, A. M.; Lewis, N. S.;
4
5 Schaak, R. E. Nanostructured Nickel Phosphide as an Electrocatalyst for the Hydrogen Evolution
6
7 Reaction, *J. Am. Chem. Soc.* **2013**, *135*, 9267–9270.

8
9
10 (19) Liang, H.; Gandi, A. N.; Xia, C.; Hedhili, M. N.; Anjum, D. H.; Schwingenschlögl, U.;
11
12 Alshareef, H. N. Amorphous NiFe-OH/NiFeP Electrocatalyst Fabricated at Low Temperature for
13
14 Water Oxidation Applications, *ACS Energy Lett.* **2017**, *2*, 1035–1042.

15
16 (20) Carenco, S.; Portehault, D.; Boissiere, C.; Mezailles, N.; Sanchez, C. Nanoscaled Metal
17
18 Borides and Phosphides: Recent Developments and Perspectives, *Chem. Rev.* **2013**, *113*, 7981–
19
20 8065.

21
22 (21) Surendranath, Y.; Dincă, M.; Nocera, D. G. Electrolyte-dependent electrosynthesis and
23
24 activity of cobalt-based water oxidation catalysts, *J. Am. Chem. Soc.* **2009**, *131*, 2615–2620.

25
26 (22) Ge, R.; Du, H.; Tao, K.; Zhang, Q.; Chen, L. Cobalt-borate nanoarray: an efficient and
27
28 durable electrocatalyst for water oxidation under benign conditions, *ACS Appl. Mater. Interfaces*
29
30 **2017**, *9*, 15383–15387.

31
32 (23) He, C.; Wu, X.; He, Z. Amorphous nickel-based thin film as a Janus electrocatalyst for
33
34 water splitting, *J. Phys. Chem. C* **2014**, *118*, 4578–4584.

35
36 (24) Suryawanshi, U. P.; Suryawanshi, M. P.; Ghorpade, U. V.; Shin, S. W.; Kim, J.; Kim, J. H.
37
38 An earth-abundant, amorphous cobalt-iron-borate (Co-Fe-B_i) prepared on Ni foam as highly
39
40 efficient and durable electrocatalysts for oxygen evolution, *Appl. Surf. Sci.* **2019**, *495*, 143462.

41
42 (25) Chen, H.; Ouyang, S.; Zhao, M.; Li, Y.; Ye, J. Synergistic Activity of Co and Fe in
43
44 Amorphous Co_x-Fe-B Catalyst for Efficient Oxygen Evolution Reaction, *ACS Appl. Mater.*
45
46 *Interfaces* **2017**, *9*, 40333–40343.

1
2
3 (26) Yu, L.; Zhou, H.; Sun, J.; Qin, F.; Yu, F.; Bao, J.; Yu, Y.; Chen, S.; Ren, Z. Cu nanowires
4 shelled with NiFe layered double hydroxide nanosheets as bifunctional electrocatalysts for
5 overall water splitting, *Energy Environ. Sci.* **2017**, *10*, 1820–1827.
6
7

8
9
10 (27) Suryawanshi, M. P.; Ghorpade, U. V.; Shin, S. W.; Suryawanshi, U. P.; Jo, E.; Kim, J. H.
11 Hierarchically Coupled Ni: FeOOH Nanosheets on 3D N-Doped Graphite Foam as Self-
12 Supported Electrocatalysts for Efficient and Durable Water Oxidation, *ACS Catal.* **2019**, *9*,
13 5025–5034.
14
15
16
17

18
19 (28) Ma, X.; Ma, M.; Liu, D.; Hao, S.; Qu, F.; Du, G.; Asiri, X. Sun, Core–Shell-Structured
20 NiS₂@Ni-B_i Nanoarray for Efficient Water Oxidation at Near-Neutral pH, *ChemCatChem* **2017**,
21 9, 3138–3143.
22
23
24
25

26 (29) Ji, X.; Hao, S.; Qu, F.; Liu, J.; Du, G.; Asiri, A. M.; Chen, L.; Sun, X. Core–shell
27 CoFe₂O₄@Co–Fe–B_i nanoarray: a surface-amorphization water oxidation catalyst operating at
28 near-neutral pH, *Nanoscale* **2017**, *9*, 7714–7718.
29
30
31
32

33 (30) Xie, L.; Qu, F.; Liu, Z.; Ren, X.; Hao, S.; Ge, R.; Du, G.; Asiri, A. M.; Sun, X.; Chen, L. In
34 situ formation of a 3D core/shell structured Ni₃N@Ni–B_i nanosheet array: an efficient non-
35 noble-metal bifunctional electrocatalyst toward full water splitting under near-neutral conditions,
36 *J. Mater. Chem. A* **2017**, *5*, 7806–7810.
37
38
39
40
41

42 (31) Yang, L.; Xie, L.; Ge, R.; Kong, R.; Liu, Z.; Du, G.; Asiri, A. M.; Yao, Y.; Luo, Y. Core–
43 Shell NiFe-LDH@NiFe-B_i Nanoarray: In Situ Electrochemical Surface Derivation Preparation
44 toward Efficient Water Oxidation Electrocatalysis in near-Neutral Media, *ACS Appl. Mater.*
45 *Interfaces* **2017**, *9*, 19502–19506.
46
47
48
49
50
51
52
53
54
55
56
57
58
59
60

1
2
3 (32) Xie, C.; Wang, Y.; Yan, D.; Tao, L.; Wang, S. In situ growth of cobalt@cobalt-borate core–
4 shell nanosheets as highly-efficient electrocatalysts for oxygen evolution reaction in
5 alkaline/neutral medium, *Nanoscale* **2017**, *9*, 16059–16065.
6
7

8
9
10 (33) Xiao, C.; Li, Y.; Lu, X.; Zhao, C. Bifunctional Porous NiFe/NiCo₂O₄/Ni Foam Electrodes
11 with Triple Hierarchy and Double Synergies for Efficient Whole Cell Water Splitting, *Adv.*
12 *Funct. Mater.* **2016**, *26*, 3515–3523.
13
14

15
16 (34) Yuan, C.; Li, J.; Hou, L.; Zhang, X.; Shen, L.; Lou, X. W. Ultrathin Mesoporous NiCo₂O₄
17 Nanosheets Supported on Ni Foam as Advanced Electrodes for Supercapacitors, *Adv. Funct.*
18 *Mater.* **2012**, *22*, 4592–4597.
19
20

21
22 (35) Li, Y.; Hasin, P.; Wu, Y. Ni_xCo_{3-x}O₄ Nanowire Arrays for Electrocatalytic Oxygen
23 Evolution, *Adv Mater.* **2010**, *22*, 1926–1929.
24
25

26
27 (36) Wang, Q.; Wang, X.; Liu, B.; Yu, G.; Hou, X.; Chen, D.; Shen, G. NiCo₂O₄ nanowire
28 arrays supported on Ni foam for high-performance flexible all-solid-state supercapacitors, *J.*
29 *Mater. Chem. A* **2013**, *1*, 2468–2473.
30
31

32
33 (37) Lu, X.; Zhao, C. Electrodeposition of hierarchically structured three-dimensional nickel–
34 iron electrodes for efficient oxygen evolution at high current densities, *Nat. Commun.* **2015**, *6*,
35 6616.
36
37

38
39 (38) Zhang, H.; Li, X.; Hähnel, A.; Naumann, V.; Lin, C.; Azimi, S.; Schweizer, S. L.;
40 Maijenburg, A. W.; Wehrspohn, R. B. Bifunctional heterostructure assembly of NiFe LDH
41 nanosheets on NiCoP nanowires for highly efficient and stable overall water splitting, *Adv.*
42 *Funct. Mater.* **2018**, *28*, 1706847.
43
44
45
46
47
48
49
50
51
52
53
54
55
56
57
58
59
60

1
2
3 (39) Sivanantham, A.; Ganesan, P.; Shanmugam, S. Hierarchical NiCo₂S₄ Nanowire Arrays
4 Supported on Ni Foam: An Efficient and Durable Bifunctional Electrocatalyst for Oxygen and
5 Hydrogen Evolution Reactions, *Adv. Funct. Mater.* **2016**, *26*, 4661–4672.
6
7

8
9
10 (40) Wang, Z.; Zeng, S.; Liu, W.; Wang, X.; Li, Q.; Zhao, Z.; Geng, F. Coupling Molecularly
11 Ultrathin Sheets of NiFe-Layered Double Hydroxide on NiCo₂O₄ Nanowire Arrays for Highly
12 Efficient Overall Water-Splitting Activity, *ACS Appl. Mater. Interfaces* **2017**, *9*, 1488–1495.
13
14

15
16 (41) Liu, Y.; Bai, Y.; Han, Y.; Yu, Z.; Zhang, S.; Wang, G.; Wei, J.; Wu, Q.; Sun, K. Self-
17 Supported Hierarchical FeCoNi-LTH/NiCo₂O₄/CC Electrodes with Enhanced Bifunctional
18 Performance for Efficient Overall Water Splitting, *ACS Appl. Mater. Interfaces* **2017**, *9*,
19 36917–36926.
20
21
22
23
24

25
26 (42) Chen, R.; Wang, H.; Miao, J.; Yang, H.; Liu, B. A flexible high-performance oxygen
27 evolution electrode with three-dimensional NiCo₂O₄ core-shell nanowires, *Nano Energy* **2015**,
28 *11*, 333–340
29
30
31

32
33 (43) Liang, H.; Li, L.; Meng, F.; Dang, L.; Zhuo, J.; Forticaux, A.; Wang, Z.; Song J. Porous
34 two-dimensional nanosheets converted from layered double hydroxides and their applications in
35 electrocatalytic water splitting, *Chem. Mater.* **2015**, *27*, 5702-5711.
36
37
38

39
40 (44) Li, Y.; Guo, S.; Jin, T.; Wang, Y.; Cheng, F.; Jiao, L. Promoted synergy in core-branch
41 CoP@NiFe–OH nanohybrids for efficient electrochemical-/ photovoltage-driven overall water
42 splitting, *Nano Energy* **2019**, *63*, 103821.
43
44
45

46
47 (45) Li, H. B.; Yu, M. H.; Wang, F. X.; Liu, P. Liang, Y.; Xiao, J.; Wang, C. X.; Tong, Y. X.;
48 Yang, G. W. Amorphous nickel hydroxide nanospheres with ultrahigh capacitance and energy
49 density as electrochemical pseudocapacitor materials, *Nat. Commun.* **2013**, *4*, 1894.
50
51
52
53
54
55
56
57
58
59

1
2
3 (46) Ma, F. -X.; Yu, L.; Xu, C.; Lou, X. W. Self-supported formation of hierarchical NiCo₂O₄
4 tetragonal microtubes with enhanced electrochemical properties, *Energy Environ. Sci.* **2016**, *9*,
5 862-866.
6
7

8
9
10 (47) Umeshbabu, E.; Rajeshkhanna, G.; Justin, P.; Ranga Rao, G. Synthesis of mesoporous
11 NiCo₂O₄-rGO by a solvothermal method for charge storage applications, *RSC Adv.* **2015**, *5*,
12 66657-66666.
13
14

15
16 (48) Ge, X.; Gu, C. D.; Wanga, X. L.; Tua, J. P. Ionothermal synthesis of cobalt iron layered
17 double hydroxides (LDHs) with expanded interlayer spacing as advanced electrochemical
18 materials, *J. Mater. Chem. A* **2014**, *2*, 17066-17076.
19
20

21 (49) Liu, G.; He, D.; Yao, R.; Zhao, Y.; Wang, M.; Li, N.; Li, J. Amorphous CoFeBO
22 nanoparticles as highly active electrocatalysts for efficient water oxidation reaction, *International*
23 *journal of hydrogen energy*, **2018**, *43*, 6138-6149.
24
25

26 (50) Xiao, C.; Lu, X.; Zhao, C. Unusual synergistic effects upon incorporation of Fe and/or Ni
27 into mesoporous Co₃O₄ for enhanced oxygen evolution, *Chem. Commun.*, **2014**, *50*, 10122-10125
28
29

30 (51) Burke, M. S.; Kast, M. G.; Trotochaud, L.; Smith, A. M.; Boettcher, S. W. Cobalt-Iron
31 (Oxy)hydroxide Oxygen Evolution Electrocatalysts: The Role of Structure and Composition on
32 Activity, Stability, and Mechanism, *J. Am. Chem. Soc.*, **2015**, *137*, 10, 3638-3648.
33
34

35 (52) Chen, P.; Xu, K.; Zhou, T.; Tong, Y. Wu, J.; Cheng, H.; Lu, X.; Ding, H.; Prof. Wu, C.;
36 Prof. Xie, Y. Strong-coupled cobalt borate nanosheets/graphene hybrid as electrocatalyst for
37 water oxidation under both alkaline and neutral conditions, *Angew. Chem. Int. Ed.* **2016**, *55*,
38 2488-2492.
39
40

41 (53) Haiqing, Z.; Fang, Y.; Jingying, S.; Ran, H.; Shuo, C.; Ching-Wu, C.; Zhifeng, R. Highly
42 active catalyst derived from a 3D foam of Fe(PO₃)₂/Ni₂P for extremely efficient water oxidation,
43
44
45
46
47
48
49
50

1
2
3 *PNAS* **2017**, 114 (22), 5607-5611
4

5 (54) Shinagawa, T.; Garcia-Esparza, A. T.; Takanabe, K. Insight on Tafel slopes from a
6 microkinetic analysis of aqueous electrocatalysis for energy conversion, *Sci. Rep.* **2015**, *5*,
7
8 13801.
9

10 (55) Huang, Z.; Chen, Z.; Chen, Z.; Lv, C.; Humphrey, M. G.; Zhang, C. Cobalt phosphide
11 nanorods as an efficient electrocatalyst for the hydrogen evolution reaction, *Nano Energy* **2014**,
12
13 *9*, 373-382.
14
15
16
17

18 (56) Yu, F.; Zhou, H.; Zhu, Z.; Sun, J.; He, R.; Bao, J.; Chen, S.; Ren, Z. Three-Dimensional
19 Nanoporous Iron Nitride Film as an Efficient Electrocatalyst for Water Oxidation, *ACS Catal.*
20
21 **2017**, *7*, 2052-2057.
22
23
24
25

26 (57) Xu, X.; Su, C.; Zhou, W.; Zhu, Y.; Chen, Y.; Shao, Z. Co-doping Strategy for Developing
27 Perovskite Oxides as Highly Efficient Electrocatalysts for Oxygen Evolution Reaction, *Adv. Sci.*
28
29 **2016**, *3*, 1500187.
30
31
32

33 (58) Ryu, J.; Jung, N.; Jang, J. H.; Kim, H. J.; Yoo, S. J. In Situ Transformation of Hydrogen-
34 Evolving CoP Nanoparticles: Toward Efficient Oxygen Evolution Catalysts Bearing Dispersed
35 Morphologies with Co-oxo/hydroxo Molecular Units, *ACS Catal.* **2015**, *5*, 4066-4074.
36
37
38
39
40
41
42
43
44
45
46
47
48
49
50
51
52
53
54
55
56
57
58
59
60

Table of Contents Entry

